Nano Energy 126 (2024) 109607

Contents lists available at ScienceDirect

Nano Energy

journal homepage: www.elsevier.com/locate/nanoen

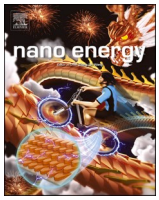

Full paper

High mass loading potassium ion stabilized manganese dioxide nanowire forests for rechargeable Zn batteries

Qiang Chen [a,b,1], Jiantao Li [c,*,1], Cong Liao [a], Wenlong Liang [b], Xuan Lou [b], Ziang Liu [a], Jianli Zhang [b], Yiping Tang [b], Liqiang Mai [a], Liang Zhou [a,*], Khalil Amine [c,*]

[a] State Key Laboratory of Advanced Technology for Materials Synthesis and Processing, Wuhan University of Technology, Wuhan 430070, China
[b] College of Material Science and Engineering, Zhejiang University of Technology, Hangzhou 310014, China
[c] Chemical Sciences and Engineering Division, Argonne National Laboratory, Lemont, IL 60439, USA

ARTICLE INFO

Keywords:
High mass loading
Manganese dioxide
Zn batteries
Flexible devices

ABSTRACT

Manganese dioxide (MnO_2) represents an ideal cathode material for rechargeable aqueous Zn batteries due to its high theoretical capacity (308 mAh g^{-1}), suitable potential (1.4 V *vs.* Zn^{2+}/Zn), natural abundance, and negligible toxicity. However, the capacity and rate capability of MnO_2 deteriorate significantly in thick electrodes owing to its low electrical and ionic conductivities. Herein, we report the design of high mass loading potassium ion stabilized α-MnO_2 ($K_{0.133}MnO_2$) nanowire forests on carbon cloth through a seed-assisted hydrothermal method for Zn batteries. The vertically aligned $K_{0.133}MnO_2$ nanowire forests with uninterrupted charge transport afford a high area capacity of 3.54 mAh cm^{-2} and a capacity retention of 79.2 % over 1000 cycles in aqueous electrolyte. Moreover, the high area capacity and cyclability can be readily transferred to quasi-solid-state devices.

1. Introduction

Aqueous rechargeable zinc batteries (ARZBs) have been identified as a promising choice for grid-scale energy storage owing to their intrinsic safety and low cost [1–5]. The cathode, which stores zinc ions reversibly, determines the energy storage capability of ARZBs. A number of cathode materials have been reported in the literature, including manganese oxides [1,2,6–9], vanadium oxides [10,11], manganates [12], vanadate [13–15], Prussian blue analogues [16–19], and polyanionic compounds [20]. Among these options, manganese dioxide (MnO_2) has become the predominant choice of RAZB cathode material owing to its high theoretical capacity (308 mAh g^{-1}), suitable potential (1.4 V *vs.* Zn^{2+}/Zn), natural abundance, and negligible toxicity [2,21–23]. Despite the multiple merits, aqueous rechargeable Zn/MnO_2 batteries are plagued by severe capacity fading due to the dissolution of Mn^{2+} in electrolyte. By introducing a certain concentration of Mn^{2+} into the electrolytes, the dissolution of Mn^{2+} can be effectively suppressed and Zn/MnO_2 batteries with excellent cyclability can be achieved [2]. However, such excellent performance can only be achieved at relatively low mass loadings. Increasing the mass loading always results in deteriorated capacity and rate capability owing to the low electrical and ionic conductivities.

In general, the MnO_2 electrodes require a small of active materials (usually less than 0.5 mg cm^{-2}) or the use of thin film structures to achieve satisfactory electrochemical performance [24–27]. In fact, low active material mass loading will restrict energy storage, which limits its commercial applications in high energy storage/conversion devices [28]. To achieve a viably commercial energy storage device, the payload of the active materials would need to reach ~ 10 mg cm^{-2} [29–31]. Nevertheless, the increasing film thickness and mass loading seriously restrict the energy storage of charge [32,33], which is primarily ascribed to the poor mechanical characteristics, slow ion transport, and poor electrical conductivity of the active materials. Usually, constructing three-dimensional (3D) nanometer structure electrodes and building conductive connections are the efficient methods to improve the electrochemical properties of high mass loading materials.

Herein, we design a flexible quasi-solid-state (QSS) Zn//$K_{0.133}MnO_2$ battery using a ultrahigh mass loading $K_{0.133}MnO_2$ (KMO) cathode and a Zn nanosheets array anode. The K content tunnel-type α-MnO_2 nanowires (KMO NWs) were formed on carbon cloth (CC) substrate via a

* Corresponding authors.
E-mail addresses: jiantao.li@anl.gov (J. Li), liangzhou@whut.edu.cn (L. Zhou), amine@anl.gov (K. Amine).
[1] These authors contribute equally to this work.

https://doi.org/10.1016/j.nanoen.2024.109607

Available online 19 April 2024
2211-2855/Published by Elsevier Ltd.

seed-assisted hydrothermal method. Zn nanosheets arrayas the anode was obtained by electrochemical deposition on carbon cloth. Our assembled Zn//KMO battery can exhibit an ultrahigh area capacity of 3.6 mA h cm^{-2} (~180 mA h g^{-1}) at a current density of 1 mA cm^{-2} (~0.05 A g^{-1}) in aqueous electrolyte. Moreover, the rechargeable Zn//KMO battery owns an extraordinary capacity retention of 83.3 % after 500 cycles with a current density of 1 mA cm^{-2}. More importantly, when assembled into a QSS device, it still affords a preeminent capacity of 3.0 mA h cm^{-2} (150 mA h g^{-1}). Additionally, this flexible Zn//KMO battery achieves an unprecedented energy density of 198.6 W h kg^{-1} (39.72 mW h cm^{-3}), and a peak power density of 118.8 kW kg^{-1} (23.76 mW cm^{-3}), outperforming most recently reported flexible energy-storage devices. This work puts forward a promising strategy to rationally design and fabricate remarkable energy/power density Zn//KMO battery, which holds great promise in energy storage/conversion systems.

2. Results and discussion

2.1. Synthesis and characterization of KMO nanowires

The growth of potassium-ion stabilized MnO_2 (KMO) is realized by a seed-assisted hydrothermal method. It is difficult to grow high mass loading active substances on the surface of carbon cloth (CC) owing to its hydrophobic nature. Therefore, a thin seed layer (Figure S1, Supporting Information) is introduced before hydrothermal procedure to induce the successive growth of KMO. The X-ray diffraction (XRD, Fig. 1a) pattern of KMO displays a series of characteristic peaks at 12.8, 18.1, 28.9, 37.8, 42.2, 50.1 and 56.5°, corresponding to the (110), (200), (310), (211), (301), (411) and (600) diffractions of $K_{0.133}MnO_2$ (JCPDS No. 42–1348) [34], respectively. Inductively coupled plasma (ICP) analysis gives rise to a K/Mn molar ratio of 0.14: 1, agreeing well with the formula $K_{0.133}MnO_2$. Scanning electron microscopy (SEM, Fig. 1b – d) images clearly show that the surface of CC is uniformly covered by a layer of KMO nanowire forest. The thickness of KMO layer is determined to be 5 – 9 μm (Fig. 1c, S2). The mass loading of KMO reaches an incredible value of 20.2 mg cm^{-2}, which is much higher than most literature values. Transmission electron microscopy (TEM, Fig. 1e) images show that the KMO nanowires are approximately 30 – 100 nm in width. An individual KMO nanowire is shown in Fig. 1f. The corresponding selected area electron diffraction (SAED, insets of Fig. 1f) pattern demonstrates its single crystalline nature. High-resolution TEM image (Fig. 1g) shows clear inter-plane spacings of 0.14 nm, corresponding to the (002) lattice fringes of $K_{0.133}MnO_2$. Scanning transmission electron microscopy-energy dispersive spectroscopy (STEM-EDS, Fig. 1h) element mappings reveal that the K, Mn, and O elements are uniformly distributed in the KMO nanowire.

X-ray photoelectron spectroscopy (XPS, Figs. 1i, 1j, S3a) shows the surface composition of the KMO. The K in KMO exists as K^+, which exhibits characteristic peaks at 294.1 and 291.3 eV (Fig. 1i) [35]. The Mn 2p spectrum exhibits two $2p_{3/2}$-$2p_{1/2}$ spin-orbit doublets. The dominated doublet shows peaks at 642.3 and 654.1 eV, which can be ascribed to $2p_{3/2}$ and $2p_{1/2}$ components of Mn (IV), respectively. The second doublet presents peaks at 641.2 and 653.2 eV, corresponding to

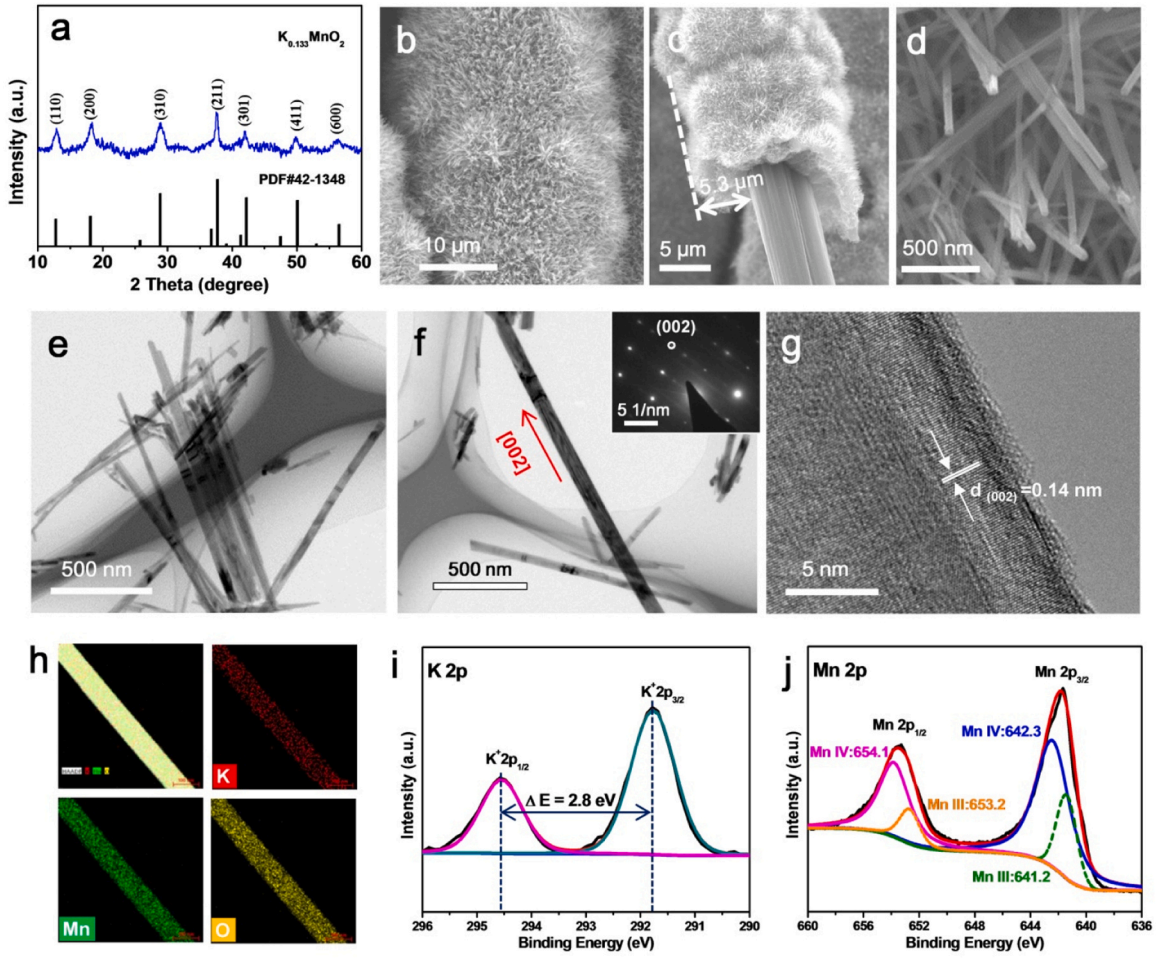

Fig. 1. Microstructural and compositional analysis of KMO. (a) XRD pattern of the KMO. (b, c, d) SEM images of the KMO at different magnification. (e, f) TEM, (The insets in panel (f) are the SAED pattern) (g) High-resolution TEM, (h) element mapping images, (i) K 2p XPS spectra and (j) Mn 2p XPS spectra of the KMO.

the $2p_{3/2}$ and $2p_{1/2}$ components of Mn (III) [36]. From the high-resolution Mn 2p spectrum, the $[Mn^{3+}]/[Mn^{4+}]$ ratio is determined to be 29.6 %. This ratio exceeds the value calculated from the formula (13.3 %). The existence of excessive Mn (III) suggests the formation of oxygen vacancies, which can be further confirmed by the O 1 s spectrum (Figure S3) with an obvious oxygen-defect peak at 531.1 eV [37]. The introduction of oxygen vacancies is favorable for electron transport and ion diffusion.

2.2. Electrochemical performance of aqueous Zn//KMO battery

The electrochemical properties of KMO are evaluated in aqueous Zn//KMO batteries. As schematically illustrated in Figure S4, a typical Zn//KMO cell is consisted of a KMO cathode, a Zn nanosheet-based anode (Figure S5), and an aqueous electrolyte containing 2.0 M $ZnSO_4$ and 0.4 M $MnSO_4$. Fig. 2**a** presents representative galvanostatic charge-discharge curves of the Zn//KMO batteries at different current densities. The discharge profiles reveal an obvious voltage platform at 1.1 – 1.4 V. An ultrahigh areal capacity of 3.54 mA h cm^{-2} can be achieved at 1 mA cm^{-2}. The Zn//KMO battery also demonstrates excellent rate performance. The discharge capacities reach 3.60, 2.86, 2.50, 2.18, 1.83, and 1.40 mA h cm^{-2} at current densities of 1, 2, 4, 6, 8, and 10 mA cm^{-2}, respectively (Fig. 2**b**).

The capacity fading associated with the dissolution of Mn^{2+} in electrolyte represents a big challenge for aqueous zinc-manganese oxide batteries. In our case, the Zn/KMO batteries demonstrates excellent cyclability owing to the introduction of $MnSO_4$ in the electrolytes, which suppresses the Mn^{2+} dissolution during cycling.[2] At a low current density of 4 mA cm^{-2}, 83.4 % of the capacity can be retained after 500 cycles (Fig. 2**c**). At a higher current density of 10 mA cm^{-2}, the Zn//KMO battery affords a capacity retention of 79.2 % over 1 000 cycles (Fig. 2**d**). It should be mentioned that the employment of Zn NSs on CC also contributes to the excellent cyclability. Traditional Zn foil anode suffers from dendrite formation (Figure S6) and inactive ZnO formation (Figure S7) during cycling, leading to unsatisfactory cyclability (Figure S8). However, such issues can be tackled by the employment of Zn NSs on CC as the anode (Figure S9).

Commercial battery devices require an active material mass loading of 10 mg cm^{-2} or even higher. In most previous studies, the active material mass loading is less than 7 mg cm^{-2}. In our case, the mass loading of KMO can be facilely tuned from 0.92 to 23.8 mg cm^{-2} by varying the hydrothermal reaction time from 0.5 to 4 h (Figure S10). The gravimetric capacity of KMO is plotted as a function of mass loading (Fig. 2**e**). As expected the gravimetric capacity decreases monotonously from 217.4 to 52.6 mAh g^{-1} with the increase of mass loadings from 0.92 to 16.4 mg cm^{-2}. This may caused by the increased barriers for ion diffusion and electron transport in thick electrodes. Surprisingly, the gravimetric capacity increases sharply from 52.6 to 175.2 mAh g^{-1} with the increase of mass loading from 16.4 to 20.2 mg cm^{-2}. Such sharp increase in capacity is associated with the difference in morphology. The KMO samples with mass loadings of 0.92 – 15.4 mg cm^{-2} (corresponding to reaction times of 0.5–2.5 h) show a dense nanosheet morphology. However, the samples with mass loadings of 20.2 – 23.8 mg cm^{-2} (corresponding to reaction times of 3.5–4 h) show a nanowire forest morphology. Compared to the dense nanosheets, the nanowire forests are more advantageous in ion diffusion. The areal capacity of KMO as a function of mass loading is also determined. A high peak areal capacity of 3.54 mAh cm^{-2} can be obtained at a mass loading of 20.2 mg cm^{-2}.

To investigate the effect of specific surface area on electrode materials, we collected Brunauer-Emmett-Teller (BET) data under different mass loads. As shown in Figure S11, there was no significant change in the specific surface area when the load was below 15 mg cm^{-2}. When the mass load reaches 20.2 mg cm^{-2}, the specific surface area increases to 34.06 m^2 g^{-1}, and the mass load further increases to 23.8 mg cm^{-2}, and the specific surface area decreases to 30.01 m^2 g^{-1}. The above results indicate that the reason for the optimal performance at a mass load of 20.2 mg cm^{-2} is related to its larger specific surface area.

Fig. 2**f** compares the KMO with recently reported RAZB cathode materials in terms of mass loading, areal capacity, and discharge voltage platform. Noteworthy, the KMO possesses the highest mass loading and areal capacity. In addition, the KMO displays a relatively high average discharge voltage of 1.3 V, which is similar to manganese dioxide.

2.3. Flexible QSS Zn//KMO battery

The QSS rechargeable Zn//KMO battery with a sandwich structure is

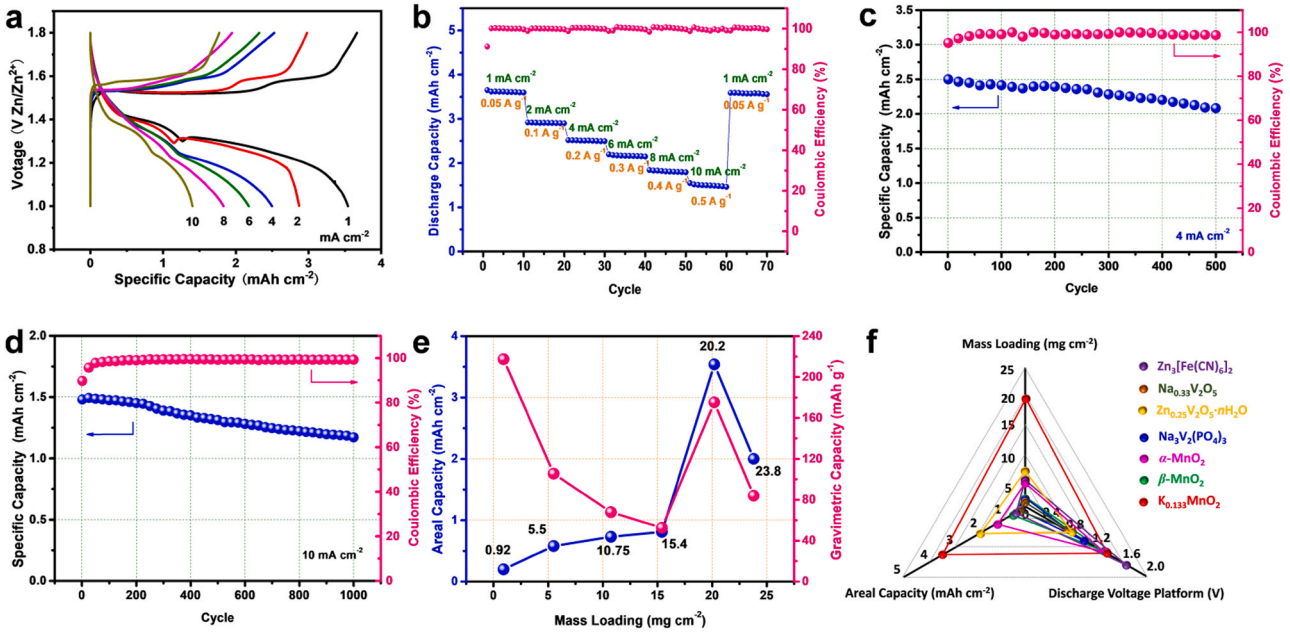

Fig. 2. Performances of aqueous Zn//KMO batteries. (a) Galvanostatic charge-discharge curves of the Zn//KMO battery at different current densities. (b) Rate performance of the Zn//KMO. (c, d) Cycling performance of the Zn//KMO battery at different current densities. (e) Areal capacity and gravimetric capacity of the KMO at a current density of 1 mA cm^{-2} as a function of mass loading. (f) Performance comparison of the KMO with other cathode materials reported elsewhere.

assembled with a flexible CC supported Zn NS anode, a KMO cathode, a gel electrolyte, and an NKK (Nippon Kodoshi Corporation) separator (Fig. 3**a**). Interestingly, the Zn//KMO battery can be assembled in an open-air environment, which is ideal for large-scale production. Fig. 3**b** presents the GCD curves of the QSS Zn//KMO battery at various current densities. The QSS Zn//KMO battery achieved a prominent discharge capacity of 3.03 mAh cm^{-2} (150.1 mAh g^{-1}) at 1 mA cm^{-2}. Even at a high current density of 5 mA cm^{-2}, a reversible capacity of 1.02 mAh cm^{-2} (50.5 mAh g^{-1}) can be obtained. Moreover, this QSS Zn//KMO battery possesses promising long-term durability, displaying a remarkable capacity retention of 92.3 % after 350 cycles at 4 mA cm^{-2} (Fig. 3**c**). Fig. 3**d** displays the discharge curves under flat, bent, and twisted testing conditions. Negligible difference in discharge capacity and voltage platform can be observed for these three states.

Figure S12a compares the power/energy densities of the Zn//KMO battery with previous works. The aqueous Zn//KMO battery demonstrates a peak energy density of 396.7 Wh kg^{-1} and peak power density of 144.1 kW kg^{-1} (based on the mass of KMO cathode). As for the QSS Zn//KMO battery, it affords a peak energy density of 198.8 Wh kg^{-1} and peak power density of 118.8 kW kg^{-1}. Such an energy density is higher than most recently developed ARZBs, such as Zn//α-MnO_2 [20], Zn//NiCoAl LDH [38], Zn//$KCuFe(CN)_6$ [17], Zn//$Zn_3Fe(CN)_6$ [18], Zn//$NiCo_2O_4$ [39], and Zn//Co_3O_4@NiO [40] batteries. In addition, the Zn//KMO battery manifests a maximum volumetric energy density of 39.7 mWh cm^{-3} and peak power density of 23.8 mW cm^{-3}. Considering the total volume of the battery, the QSS Zn//KMO battery reaches a peak volumetric energy density of 10.9 mWh cm^{-3} and peak power density of 6.5 mW cm^{-3}, indicating the great potential for commercial applications (Figure S12b).

To exemplify the practical application of the flexible QSS Zn//KMO batteries, three cells are connected in series to power a neon sign consisting of 42 light emitting diodes (LEDs). After being charged at 2 mA cm^{-2} for 20 min, the cells illuminate the neon sign with a dazzling brightness under different condition and the LEDs continue to shine for 90 min (Figure S13 and Supplementary movie 1). In addition, the cells are able to work under complex environment, such as bending, extrusion, and in water conditions, even power a neon sign consisting of 60 LEDs (Figure S14, Supplementary movie 1 and Supplementary movie 2). The above results clearly indicate that the flexible QSS Zn//KMO battery possesses prominent performance, suggesting its promising application in wearable electronics.

2.4. Charge storage mechanism in KMO nanowires

To reveal the charge storage mechanism of KMO, *ex-situ* XRD is conducted. Fig. 4**a** shows the *ex-situ* XRD patterns of KMO during charge-discharge with the corresponding GCD curve shown in Fig. 4**b**. The XRD pattern shows little change during charge-discharge except for the reversible appearance of three small peaks. The three small peaks become more obvious when discharging, and gradually disappear when charging. The XRD diffraction peaks at 21.1°, 32.9°, and 34.0° are attributed to $Zn_4SO_4(OH)_6 \bullet nH_2O$ (JCPDS No. 35–0910). [34] Fig. 4**c** shows the change of KMO morphology during charging and discharging. After discharging, $Zn_4SO_4(OH)_6 \bullet nH_2O$ with a flaky structure was deposited on the surface of KMO nanowires, which disappeared after charging. Therefore, no noticeable structural collapse can be detected during the charge-discharge. The *ex-situ* XRD results demonstrate unambiguously that the charge storage in KMO is mainly through H^+ intercalation/de-intercalation. During the discharge process, H^+ intercalation into the structure leads to the enrichment of OH^- on the surface of the KMO electrode and reacts with electrolytes (Zn^{2+} and SO_4^{2-}) to deposit $Zn_4SO_4(OH)_6 \bullet nH_2O$ nanosheets. Based on the *ex-situ* XRD and SEM results, a charge storage mechanism for KMO is proposed (Fig. 4**d**). It should be noted that the charge storage mechanism of KMO is quite different from that of MnO_2, which usually involves the conversion of MnO_2 to MnOOH ($MnO_2 + H_2O + e^- \leftrightarrow MnOOH + OH^-$) or $ZnMn_2O_4$ ($MnO_2 + Zn^{2+} + 2\,e^- \leftrightarrow ZnMn_2O_4$). Considering the structural similarity of KMO and α-MnO_2, the difference in mechanism may be ascribed to the

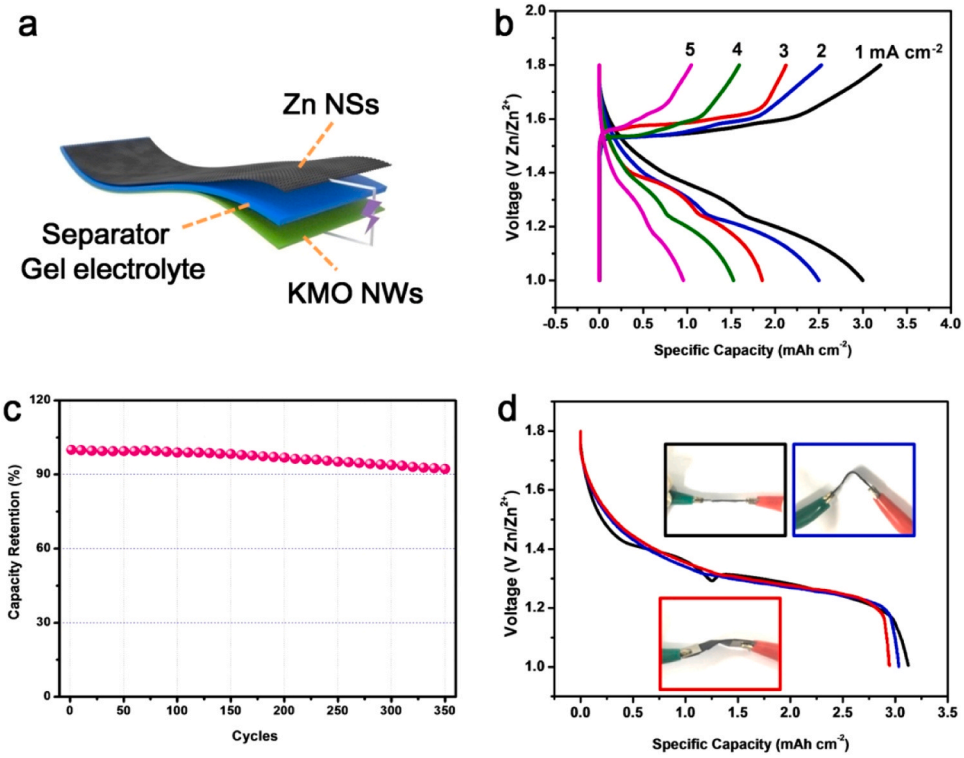

Fig. 3. Performance of flexible QSS Zn//KMO battery. (a) Schematic illustration for the structure of flexible QSS Zn//KMO battery. (b) Galvanostatic charge-discharge (GCD) curves of the QSS Zn//KMO battery at various current densities. (c) Cycling performance of the QSS Zn//KMO battery at 4 mA cm^{-2}. (d) Discharge curves at 1 mA cm^{-2} of the flexible QSS Zn/KMO battery under flat, bent, and twisted conditions.

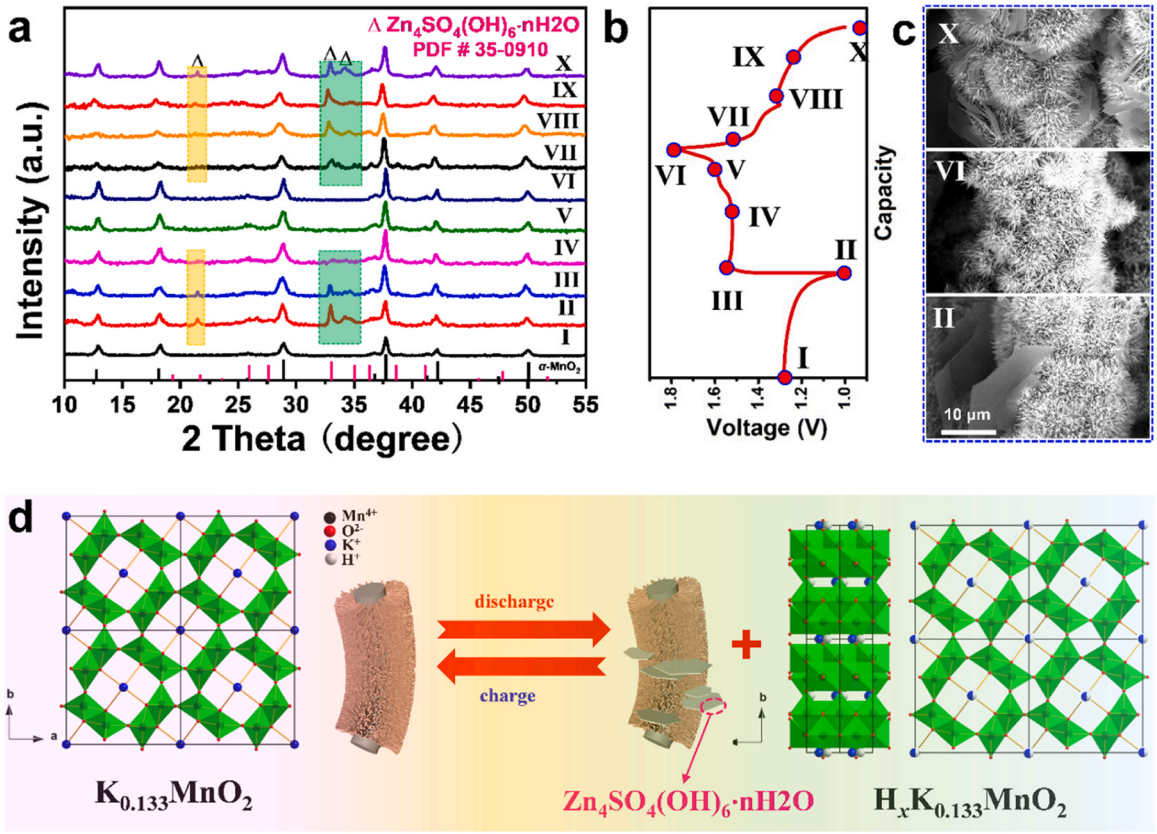

Fig. 4. Charge storage mechanism of KMO. (a) The *ex-situ* XRD patterns of KMO at different charge/discharge states, and the corresponding (b) GCD curves and (c) SEM images at 1 mA cm^{-2}. (d) Schematic illustration of the charge storage mechanism in KMO.

existence of K^+ in the tunnels of α-MnO_2, which stabilizes the structure.

There markable electrochemical property of KMO can be ascribed to the following reasons. (I) The K^+-stabilized manganese dioxide ($K_{0.133}MnO_2$) enables a new H^+ intercalation/de-intercalation combined with $Zn_4SO_4(OH)_6{\bullet}nH_2O$ deposition/stripping reaction mechanism and ideal cyclability. (II) The growth of KMO nanowire forests on CC provides uninterrupted charge transport in thick electrodes and enables high areal specific capacity.

3. Conclusion

In conclusion, a highly flexible rechargeable Zn//KMO battery with extraordinary properties was designed. The ultrahigh mass loading (~20 mg cm^{-2}) K content α-MnO_2 (KMO) nanowires were formed on flexible carbon cloth as cathode material. Zn nanosheets (Zn NSs), which are connected to each other by quantum dots as the anode, were obtained by the one-step electrodeposition method on carbon cloth. When tested in aqueous electrolyte, our Zn//KMO battery not only has a prominent capacity of 3.54 mA h cm^{-2} (175.2 mA h g^{-1}) but also displays supernormal long durability with capacity retention of 79.2 % after 1 000 cycles. When applied in QSS devices, our Zn//KMO battery also affords an excellent peak energy density of 198.6 Wh kg^{-1} (39.72 mW h cm^{-3}) at a peak power density of 118.8 kW kg^{-1} (23.76 mW cm^{-3}), which is higher than many of ARZBs recently reported. In addition, the successful construction of flexible Zn//KMO batteries with high energy and power densities could enrich the next-generation wearable storage/conversion systems.

CRediT authorship contribution statement

Liang Zhou: Writing – review & editing, Supervision, Conceptualization. **Liqiang Mai:** Conceptualization. **Yiping Tang:** Writing – review & editing. **Jianli Zhang:** Funding acquisition. **Ziang Liu:** Formal analysis. **Xuan Lou:** Formal analysis. **Wenlong Liang:** Formal analysis. **Cong Liao:** Methodology. **Jiantao Li:** Writing – review & editing, Supervision, Conceptualization. **Qiang Chen:** Writing – original draft. **Khalil Amine:** Supervision, Conceptualization.

Declaration of Competing Interest

The authors declare no competing financial interest.

Data Availability

Data will be made available on request.

Acknowledgements

This work was supported by the National Natural Science Foundation of China (52202313, U1802254, 52202315, 52271039), and Natural Science Foundation of Zhejiang Province (LY24E020008, LZ22E010002). This work gratefully acknowledges support from the U. S. Department of Energy (DOE), Office of Energy Efficiency and Renewable Energy, Vehicle Technologies Office.

Supporting Information

Supplementary data associated with this article can be found in the online version.

Appendix A. Supporting information

Supplementary data associated with this article can be found in the online version at doi:10.1016/j.nanoen.2024.109607.

References

[1] C. Xu, B. Li, H. Du, F. Kang, Energetic zinc ion chemistry: the rechargeable zinc ion battery, Angew. Chem. Int. Ed. 51 (2012) 933–935.

[2] H. Pan, Y. Shao, P. Yan, Y. Cheng, K.S. Han, Z. Nie, C. Wang, J. Yang, X. Li, P. Bhattacharya, K.T. Mueller, J. Liu, Reversible aqueous zinc/manganese oxide energy storage from conversion reactions, Nat. Energy 1 (2016) 16039.

[3] D. Kundu, B.D. Adams, V. Duffort, S.H. Vajargah, L.F. Nazar, A high-capacity and long-life aqueous rechargeable zinc battery using a metal oxide intercalation cathode, Nat. Energy 1 (2016) 16119.

[4] F. Wang, O. Borodin, T. Gao, X. Fan, W. Sun, F. Han, A. Faraone, J.A. Dura, K. Xu, C. Wang, Highly reversible zinc metal anode for aqueous batteries, Nat. Mater. 17 (2018) 543–549.

[5] L.E. Blanc, D. Kundu, L.F. Nazar, Scientific Challenges for the Implementation of Zn-Ion Batteries, Joule 4 (2020) 771–799.

[6] X. Li, Q. Zhou, Z. Yang, X. Zhou, D. Qiu, H. Qiu, X. Huang, Y. Yu, Unraveling the role of nitrogen-doped carbon nanowires incorporated with MnO_2 nanosheets as high performance cathode for zinc-ion batteries, Energy Environ. Mater. 6 (2022) e12378.

[7] H. Yao, H. Yu, Y. Zheng, N.W. Li, S. Li, D. Luan, X.D. Lou, L. Yu, Pre-intercalation of ammonium ions in layered delta-MnO_2 nanosheets for high-performance aqueous zinc-ion batteries, Angew. Chem. Int. Ed. (2023) e202315257.

[8] Q. Chen, X. Lou, Y. Yuan, K. You, C. Li, C. Jiang, Y. Zeng, S. Zhou, J. Zhang, G. Hou, J. Lu, Y. Tang, Surface adsorption and proton chemistry of ultra-stabilized aqueous zinc-manganese dioxide batteries, Adv. Mater. (2023) 2306294.

[9] J. Jin, X. Geng, Q. Chen, T.L. Ren, A better Zn-Ion storage device: recent progress for Zn-Ion hybrid supercapacitors, Nano-Micro Lett. 14 (2022) 64.

[10] J. Ding, Z. Du, L. Gu, B. Li, L. Wang, S. Wang, Y. Gong, S. Yang, Ultrafast Zn^{2+} intercalation and deintercalation in vanadium dioxide, Adv. Mater. 30 (2018) 1800762.

[11] J. Guo, J. Liu, W. Ma, Z. Sang, L. Yin, X. Zhang, H. Chen, J. Liang, Da Yang, Vanadium oxide intercalated with conductive metal–organic frameworks with dual energy-storage mechanism for high capacity and high-rate capability Zn ion storage, Adv. Funct. Mater. 33 (2023) 2302659.

[12] M. Wang, Y. Meng, Y. Xu, N. Chen, M. Chuai, Y. Yuan, J. Sun, Z. Liu, X. Zheng, Z. Zhang, D. Li, W. Chen, Aqueous all-manganese batteries, Energy Environ. Sci. 16 (2023) 5284–5293.

[13] C. Xia, J. Guo, P. Li, X. Zhang, H.N. Alshareef, Highly stable aqueous zinc-ion storage using a layered calcium vanadium oxide bronze cathode, Angew. Chem. Int. Ed. 57 (2018) 3943–3948.

[14] N. Zhang, F. Cheng, J. Liu, L. Wang, X. Long, X. Liu, F. Li, J. Chen, Rechargeable aqueous zinc-manganese dioxide batteries with high energy and power densities, Nat. Commun. 8 (2017) 405.

[15] P. Hu, T. Zhu, X. Wang, X. Wei, M. Yan, J. Li, W. Luo, W. Yang, W. Zhang, L. Zhou, Z. Zhou, L. Mai, Highly durable $Na_2V_6O_{16}{\cdot}1.63H_2O$ nanowire cathode for aqueous zinc-ion battery, Nano. Lett. 18 (2018) 1758–1763.

[16] Y. Sun, Z. Xu, X. Xu, Y. Nie, J. Tu, A. Zhou, J. Zhang, L. Qiu, F. Chen, J. Xie, T. Zhu, X. Zhao, Low-cost and long-life Zn/Prussian blue battery using a water-in-ethanol electrolyte with a normal salt concentration, Energy Storage Mater. 48 (2022) 192–204.

[17] L. Zhang, L. Chen, X. Zhou, Z. Liu, Towards high-voltage aqueous metal-ion batteries beyond 1.5 V: the Zinc/Zinc hexacyanoferrate system, Adv. Energy Mater. 5 (2014) 1400930.

[18] A. Naveed, H. Yang, J. Yang, Y. Nuli, J. Wang, Highly reversible and rechargeable safe Zn batteries based on a triethyl phosphate electrolyte, Angew. Chem. Int. Ed. 58 (2019) 2760–2764.

[19] Q. Chen, W. Liang, Z. Tang, J. Jin, J. Zhang, G. Hou, L. Mai, Y. Tang, Aqueous ammonium ion storage materials: a structure perspective, Mater. Today 72 (2024) 359–376.

[20] D. Bin, Y. Du, B. Yang, H. Lu, Y. Liu, Y. Xia, Progress of phosphate-based polyanion cathodes for aqueous rechargeable zinc batteries, Adv. Funct. Mater. 33 (2022) 2211765.

[21] Q. Zhao, A. Song, W. Zhao, R. Qin, S. Ding, X. Chen, Y. Song, L. Yang, H. Lin, S. Li, F. Pan, Boosting the energy density of aqueous batteries via facile grotthuss proton transport, Angew. Chem. Int. Ed. 60 (2021) 4169–4174.

[22] X. Ye, D. Han, G. Jiang, C. Cui, Y. Guo, Y. Wang, Z. Zhang, Z. Weng, Q.-H. Yang, Unraveling the deposition/dissolution chemistry of MnO_2 for high-energy aqueous batteries, Energy Environ. Sci. 16 (2023) 1016–1023.

[23] Y. Zuo, T. Meng, H. Tian, L. Ling, H. Zhang, H. Zhang, X. Sun, S. Cai, Enhanced H^+ storage of a MnO_2 cathode via a MnO_2 nanolayer interphase transformed from manganese phosphate, ACS Nano 17 (2023) 5600–5608.

[24] Y. Xu, G. Zhang, J. Liu, J. Zhang, X. Wang, X. Pu, J. Wang, C. Yan, Y. Cao, H. Yang, W. Li, X. Li, Recent advances on challenges and strategies of manganese dioxide cathodes for aqueous zinc-ion batteries, Energy Environ. Mater. 6 (2023) e12575.

[25] Q. Lv, S. Wang, H. Sun, J. Luo, J. Xiao, J. Xiao, F. Xiao, S. Wang, Solid-state thin-film supercapacitors with ultrafast charge/discharge based on N-doped-carbon-tubes/Au-nanoparticles-doped-MnO_2 nanocomposites, Nano Lett. 16 (2016) 40–47.

[26] J. Li, N. Luo, L. Kang, F. Zhao, Y. Jiao, T.J. Macdonald, M. Wang, I.P. Parkin, P. R. Shearing, D.J.L. Brett, G. Chai, G. He, Hydrogen-bond reinforced superstructural manganese oxide as the cathode for ultra-stable aqueous zinc ion batteries, Adv. Energy Mater. 12 (2022) 201840.

[27] Y. Deng, H. Wang, M. Fan, B. Zhan, L.J. Zuo, C. Chen, L. Yan, Nanomicellar electrolyte to control release ions and reconstruct hydrogen bonding network for ultrastable high-energy-density Zn-Mn battery, J. Am. Chem. Soc. 145 (2023) 20109–20120.

[28] H. Yang, R. Zhu, Y. Yang, Z. Lu, Z. Chang, P. He, C. Zhu, S. Kitano, Y. Aoki, H. Habazaki, H. Zhou, Sustainable high-energy aqueous zinc–manganese dioxide batteries enabled by stress-governed metal electrodeposition and fast zinc diffusivity, Energy Environ. Sci. 16 (2023) 2133–2141.

[29] B. Yao, S. Chandrasekaran, J. Zhang, W. Xiao, F. Qian, C. Zhu, E.B. Duoss, C. M. Spadaccini, M.A. Worsley, Y. Li, Efficient 3D printed pseudocapacitive electrodes with ultrahigh MnO_2 loading, Joule 3 (2019) 459–470.

[30] C. Xu, Z. Li, C. Yang, P. Zou, B. Xie, Z. Lin, Z. Zhang, B. Li, F. Kang, C.P. Wong, An ultralong, highly oriented nickel-nanowire-array electrode scaffold for high-performance compressible pseudocapacitors, Adv. Mater. 28 (2016) 4105–4110.

[31] H. Sun, L. Mei, J. Liang, Z. Zhao, C. Lee, H. Fei, M. Ding, J. Lau, M. Li, C. Wang, X. Xu, G. Hao, B. Papandrea, I. Shakir, B. Dunn, Y. Huang, X. Duan, Three-dimensional holey-graphene/ niobia composite architectures for ultrahigh-rate energy storage, Scinece 356 (2017) 599–604.

[32] K. Wang, J. Wang, P. Chen, M. Qin, C. Yang, W. Zhang, Z. Zhang, Y. Zhen, F. Fu, B. Xu, Structural transformation by crystal engineering endows aqueous zinc-ion batteries with ultra-long cyclability, Small 19 (2023) 2300585.

[33] Q. Chen, J. Jin, Z. Kou, C. Liao, Z. Liu, L. Zhou, J. Wang, L. Mai, Zn^{2+} Pre-intercalation stabilizes the tunnel structure of MnO_2 nanowires and enables zinc-ion hybrid supercapacitor of battery-level energy density, Small 16 (2020) 2000091.

[34] P. Tozman, J.M.D. Coey, Z. Gercsi, Structure and magnetic order in Mn_8Ga_5, Acta Mater. 113 (2016) 147–154.

[35] L. Caracciolo, L. Madec, L. Madec, XPS Analysis of K-based reference compounds to allow reliable studies of solid electrolyte interphase in K-ion batteries, ACS Appl. Energy Mater. 4 (2021) 11693–11699.

[36] M.C. Biesinger, B.P. Payne, A.P. Grosvenor, L.W.M. Lau, A.R. Gerson, R.S.C. Smart, Resolving surface chemical states in XPS analysis of first row transition metals, oxides and hydroxides: Cr, Mn, Fe, Co and Ni, Appl. Surf. Sci. 257 (2011) 2717–2730.

[37] Y. Zeng, Y. Han, Y. Zhao, Y. Zeng, M. Yu, Y. Liu, H. Tang, Y. Tong, X. Lu, Advanced Ti-doped Fe_2O_3@PEDOT Core/shell anode for high-energy asymmetric supercapacitors, Adv. Energy Mater. 5 (2015) 1402176.

[38] M. Gong, Y. Li, H. Zhang, B. Zhang, W. Zhou, J. Feng, H. Wang, Y. Liang, Z. Fan, J. Liu, H. Dai, Ultrafast high-capacity NiZn battery with NiAlCo-layered double hydroxide, Energy Environ. Sci. 7 (2014) 2025–2032.

[39] X. Wang, F. Wang, L. Wang, M. Li, Y. Wang, B. Chen, Y. Zhu, L. Fu, L. Zha, L. Zhang, Y. Wu, W. Huang, An aqueous rechargeable Zn//Co_3O_4 battery with high energy density and good cycling behavior, Adv. Mater. 28 (2016) 4904–4911.

[40] Z. Lu, X. Wu, X. Lei, Y. Li, X. Sun, Hierarchical nanoarray materials for advanced nickel–zinc batteries, Inorg. Chem. Front. 2 (2015) 184–187.

Qiang Chen received his Ph.D. degree from Wuhan University of Technology in 2021. Dr. Chen as a joint training doctoral student at the National University of Singapore in 2019–2020. He is currently an associate professor of Materials Science and Engineering at the College of Materials Science and Engineering, Zhejiang University of Technology, China. His current research involves nanomaterials and devices for energy storage.

Dr. Jiantao Li is a postdoctoral appointee in the Chemical Sciences and Engineering Division at Argonne National Laboratory. He received his Ph.D. degree in Materials Science and Engineering from Wuhan University of Technology in 2019. His research focuses on electrochemical energy storage and conversion technologies, with a main focus on Li-O_2 battery and solid-state battery technologies.

Cong Liao is currently pursuing a master's degree in the School of Materials Science and Engineering at Huazhong University of Science and Technology. His research interests focus on sulfide-based all-solid-state batteries.

Wenlong Liang studied at Henan Institute of Technology in 2018 and studied as a graduate student at Zhejiang University of Technology in 2022. The current research focus is on aqueous ammonium ion batteries and aqueous ammonium ion hybrid supercapacitors.

Xuan Lou is a postgraduate student in the College of Materials Science and Engineering, Zhejiang University of Technology. His main research interests are the modification of positive electrode materials and storage mechanism of aqueous zinc-manganese dioxide batteries.

Ziang Liu received his B.S. degree in Wuhan University of Technology in 2017. He is currently working toward the Ph.D. degree at Wuhan University of Technology and his current research involves energy materials and devices.

Jianli Zhang obtained his Ph.D. (2019) in Material Science and Engineering from school of Chemical Engineering, Nanjing University of Science and Technology, China. He is currently a postdoctoral under the supervision of Professor Yiping Tang at Zhejiang University of Technology, China. His current research interest is mainly focus on energy storage materials.

Yiping Tang obtained his MS degree (2003) and Ph.D. (2007) in Material Science and Engineering from School of Materials Science and Engineering (Central South University, China) and School of Materials Science and Engineering (Shanghai Jiaotong University, China), respectively. He is currently a full professor of Materials Science and Engineering at School of Materials Science and Engineering, Zhejiang University of Technology, China. His research interests are in the fields of metal functional materials, energy storage materials, and material surface modification.

Liqiang Mai is a Chair Professor of Materials Science and Engineering at the Wuhan University of Technology (WUT), Dean of the School of Materials Science and Engineering at WUT, and Fellow of the Royal Society of Chemistry. He received his PhD from WUT in 2004 and carried out his postdoctoral research at Georgia Institute of Technology in 2006– 2007. He worked as an advanced research scholar at Harvard University in 2008–2011 and the University of California, Berkeley in 2017. His current research interests are focused on new nanomaterials for electrochemical energy storage and micro/nano energy devices.

Liang Zhou received his Ph.D. degree from Department of Chemistry, Fudan University in 2011. After graduation, he worked as a postdoctoral research fellow at Nanyang Technological University (2011–2012) and The University of Queensland (2012–2015). He is now a full professor at Wuhan University of Technology. His research interests include functional nanomaterials for electrochemical energy storage.

Dr. Khalil Amine is Argonne Distinguished Fellow and the leader of the Advanced Battery Technology team at Argonne National Laboratory, where he is responsible for directing the research and development of advanced materials and battery systems for HEV, PHEV, EV, and satellite applications. He is an adjunct professor at Stanford University. Among his many awards, Dr. Amine is the 2019 reception of the prestigious Global Energy Prize. He is a six-time recipient of the R&D 100 Award, which is considered as the Oscar of technology and innovation. He is an ECS fellow, and associate editor of the journal of Nano Energy.